DOI 10.36146/2026_05_34

Microstructure and mechanical properties of Super Duplex Stainless Steel Friction stir and Electron beam welds

C. B. Sekar, S. Vijayan, S. R. Koteswara Rao

In this investigation the mechanical and microstructural properties of Electron Beam Welded (EBW) and Friction Stir Welded (FSW) 2507 Super Duplex Stainless Steel (SDSS) welds were studied. The Super Duplex Stainless Steel has an equal proportion of the ferrite and austenite phases and the change in the proportion will lead to the changes in the microstructure which in turn affects the weldment properties. Thus, it is motivating to try to analyze, compare, and investigate the mechanical properties and microstructural aspects of the fusion (EBW) and solid state (FSW) welded SDSS2507. Both approaches have potential for high-performance applications, the findings provide insights into the suitability of EBW and FSW for SDSS 2507 applications, highlighting their potential to meet the demanding conditions in oil, gas, and marine industries. Mechanical testing, including tensile, micro hardness, impact toughness, and bend tests were used to evaluate the welded joints. The microstructural investigation of phase distribution and grain structure was carried out using optical microscope and scanning electron microscopy (SEM). Ferrite measurement revealed that the percentage of ferrite is more than the austenite phase at the center of both the welds, with EB weld metal having higher ferrite content (about 65%). The tensile test specimens failed in the weld nugget in case of friction stir welds and in the base metal in case of EB welds as can be predicted from the high hardness values exhibited by the EB weld metal. Both types of welded joints exhibited high joint efficiencies above 90%. Results indicate that both EBW and FSW produce robust joints with distinct microstructures and both can be employed for structural applications requiring high joint strength.

KEYWORDS: SUPER DUPLEX STAINLESS STEEL 2507; FSW; EBW; MICROSTRUCTURE AND MECHANICAL PROPERTIES.

INTRODUCTION

Super duplex stainless steel 2507 (SDSS) is widely used for its dual-phase microstructure, combining approximately equal parts of ferrite and austenite, resulting in high strength and corrosion resistance. This unique composition grants it superior corrosion resistance and mechanical strength, ideal for high-stress environments in industries such as offshore oil and gas, petrochemical, and chemical processing. The alloy's balanced microstructure also provides excellent resistance to pitting, stress corrosion cracking, and general corrosion in chloride-rich environments, making it particularly valuable in harsh operational conditions [1-2]. However, due to its complex phase structure, welding SDSS 2507 is challenging, as improper heat input or processing can disrupt

C. B. Sekar
Department of Mechanical Engineering, Meenakshi College of Engineering, Chennai, India.

S. Vijayan, S. R. Koteswara Rao
Department of Mechanical Engineering, Sri Sivasubramaniya Nadar College of Engineering, Chennai, India.

the delicate ferrite-austenite balance, leading to reduced mechanical performance and increased corrosion susceptibility. V. A. Hosseini et al [3] studied the impact of multiple thermal cycles during TIG welding on SDSS. The study focuses on the formation of secondary phases, such as sigma phase and nitrides, and how these phases influence both microstructure and corrosion resistance. Key findings include the identification of different thermal zones within the welded area, each exhibiting varying degrees of ferrite and secondary phase content depending on heat input. The study highlights that higher heat inputs reduce the formation of detrimental phases like nitrides by slowing the cooling rate, while multiple passes promote their formation, negatively affecting mechanical and corrosion properties [3].

Electron beam welding (EBW) and friction stir welding (FSW) have emerged as prominent methods for joining SDSS 2507, each with unique characteristics. EBW is a fusion welding process that uses a high-energy electron beam to penetrate deep into the material, enabling high welding speeds and minimal distortion due to its narrow, focused heat affected zone (HAZ). This characteristic is advantageous for SDSS, as the rapid cooling and narrow HAZ help maintain phase balance in SDSS 2507, thus preserving its mechanical properties and corrosion resistance [4-5]. EBW's ability to create precise, deep welds makes it well-suited for thick sections and high-stress components, yet some research suggests that the extreme heat of EBW may risk introducing embrittlement if not carefully controlled [6]. Z. Zhang et al investigates the impact of heat input on the microstructure and mechanical properties of duplex stainless steel (DSS) EBW welds. The study highlights how varying heat inputs influence the formation of ferrite and austenite, Cr2N precipitation, and mechanical properties like hardness and toughness. Recommended heat input is 0.46 kJ/mm for optimal properties [7].

FSW, on the other hand, is a solid-state process that joins materials without melting. By using frictional heat and mechanical stirring, FSW allows SDSS 2507 to retain its original microstructure, which is beneficial for maintaining both phase balance and material toughness. Studies have shown that FSW can improve joint integrity and extend fatigue life in duplex stainless steels, a result of its lower-temperature processing and minimized thermal stresses [8-9]. Because it limits the formation of harmful intermetallic phases, FSW is increasingly favoured for applications where corrosion resistance and mechanical strength are paramount [10]. R.A. Giorjão et al. studied the influence of FSW process parameters (spindle speed, welding speed) on SDSS 2507 welds, using tensile and bend tests for mechanical evaluation [11]. M. M. Seleman et al. investigated on the focus on various FSW tool geometries and their impact on weld quality, emphasizing tensile and hardness testing [12].

This study presents a comparative analysis of the mechanical and microstructural properties of SDSS 2507 when welded using EBW and FSW. By evaluating the hardness, tensile strength, corrosion resistance, and microstructural characteristics of each weld, we aim to offer insights in comparison of these welding processes for industry applications, contributing to the reliable and efficient use of SDSS 2507 in critical environments.

EXPERIMENTAL PROCEDURE

SDSS 2507 of 6 mm thick was employed for this investigation. Vacuum arc emission spectrometric analysis was used to determine the base metal chemical composition and the weight % of the elements present in the base metal, as displayed in table 1. The base metal tensile samples, impact toughness and bend test were made according to ATM E8-04 (ASTM, 2004), ASTM E23-07 (ASTM, 2007) and E190-92 (ASTM, 2008) standards. The mechanical properties of the base metal such as Yield strength, Tensile strength, Elongation (%), Vickers Micro-hardness and Charpy Impact Toughness are shown in table 2. For macro-structural analysis, the transverse sides of weld joints were cut, polished up to 2500 grit emery sheets and etched using 10% NaOH electrolyte etching technique. The macrographs of the welded joints were captured using a stereo zoom microscope to analyse the presence of micro or macro voids or cracks by studying the following parameters (i) penetration depth (ii) maximum width of the joints (iii) weld area produced by joints and (iv) weld zones.

Tab.1 - Chemical composition of 2507 SDSS.

Material	Weight % of elements									
	C	Mn	P	S	Si	Cu	Ni	Cr	Mo	N
SDSS 2507	0.023	0.826	0.021	0.002	0.414	0.098	6.340	25.620	3.740	0.247

Tab.2 - Mechanical properties of the base metal (measured values).

Mechanical properties	Evaluated Values
Yield strength (MPa)	704 ± 4
Tensile strength (MPa)	860 ± 7
Elongation (%) in 25mm gauge length	42 ± 1.5
Vickers Micro-hardness (HV0.5@15sec)	255 ± 8
Charpy Impact Toughness @RT (J)	63 ± 2

WELD JOINT FABRICATION

The base plate, of 100 mm long, 75 mm wide, and 6 mm thick, was machined to fabricate the EBW and FSW welds. Prior to welding, the base plate was cleaned with acetone in order to remove all the grease and debris. Square butt joints of EBW and FSW were fabricated using the optimum process parameters obtained from the trials and listed in the literature [13-14] and are shown in table 3.

Tab.3 - Welding techniques and process parameters.

Welding Process	Process Parameters
EBW	Voltage =100 Kv
	Beam current = 27 mA
	Travel speed = 600 mm/min
FSW	Tool rotation speed - 600 rpm
	Tool Traverse Speed - 25 mm/min

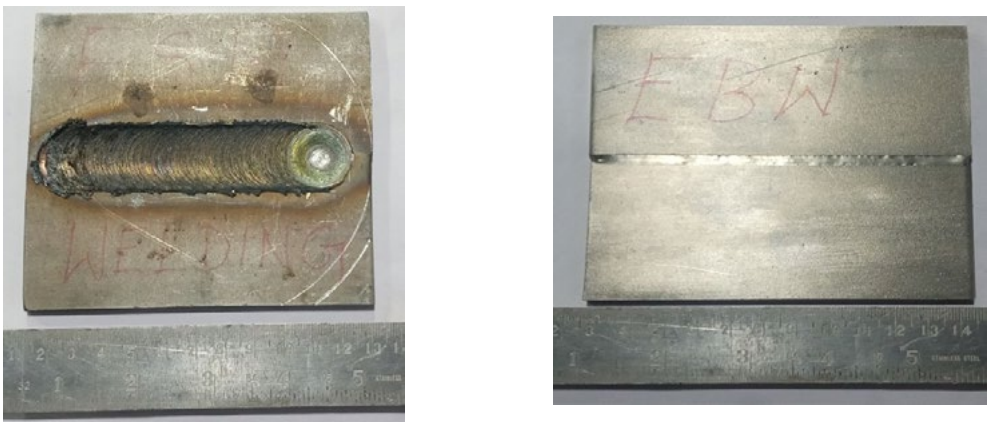

(a) FSW joint (b) EBW joint

Fig.1 - Fabricated weld joints.

RESULTS AND DISCUSSION

Micro and macro structural characterization

SEM and optical microscopy were used to examine the microstructural properties of the welded joints and base metal. Using optical microscopy, the impact of the EBW and FSW welding procedures on microstructural morphologies was thoroughly examined. In the meantime, scanning electron microscopy was used to evaluate the average grain size and grain size distribution for the EBW and FSW joints. The base metal microstructural features are shown in figure 2. Austenite (γ) and ferrite (α), two phases (dual phase), were seen in the optical microscope image [15]. The austenite and ferrite phases are denoted by the white and dark phases of the stripe type, respectively. In the dual phases, the grain thickness ranged from 12 to 20 μm, with an average of approximately 15.2 μm. Figures 3 and 4 show the grain thickness indicator and the grain thickness size distribution, respectively.

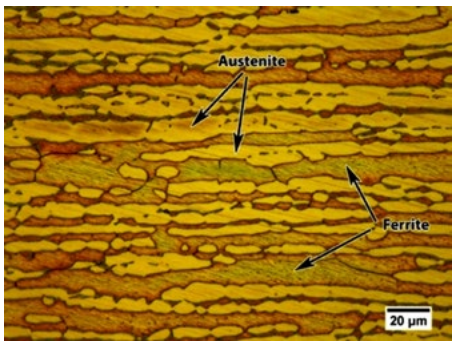

Fig.2 - Optical micrograph of 2507 SDSS (ferrite and austenite).

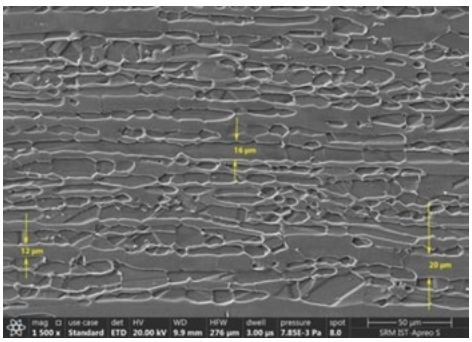

Fig.3 - Indication of grain thickness of the base metal.

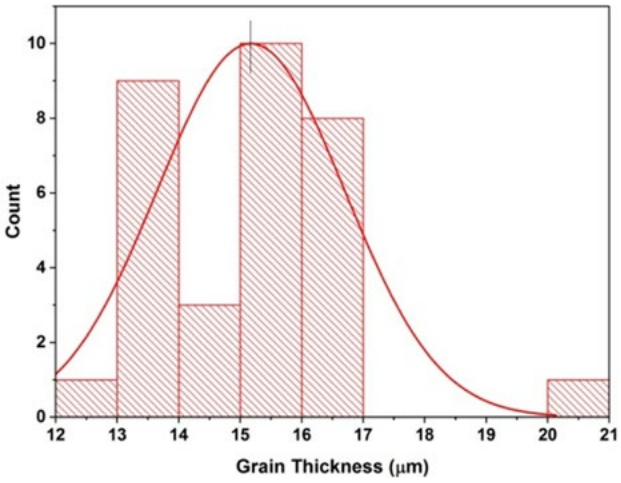

Fig.4 - Distribution of Grain Thickness in base metal.

ELECTRON BEAM WELDING (EBW)

The EBW joint macrostructure is shown in figure 5a. The fusion zone was found to have two separate zones: (i) a narrow fusion zone at the root side, and (ii) a wide fusion zone at the face side. The keyhole welding causing significant variation in cooling rates at the face and root sides of the EBW joint during solidification is responsible for this shape of fusion zone. The face side of the fusion zone has a bead width of 5.8 mm, whereas the root side has a low bead width of 1.5 mm. For the EBW joint, the measured weld area was 14.7 mm^2. The fusion zone microstructure at the EBW joint face side is seen in figure 5b. It has columnar grains growing from the top surface of the weld and the base metal (epitaxial growth). Additionally, intragranular austenite was observed at the face side of the fusion zone which has also been observed by other investigators [16]. The morphology of the root side of the fusion zone contained large number of finer equiaxed grains. Howe-

ver, the absence of Widmannstätten austenite was noted, and the ferrite grains are tiny. The grain size distribution and the enlarged image of the face side of the fusion zone are shown in figures 6a and 6b, respectively. Figure 6b shows that the average grain size at the face side of the fusion zone is 108 μm. The root side of the fusion zone is shown in magnified view in figures 6c and 6d.

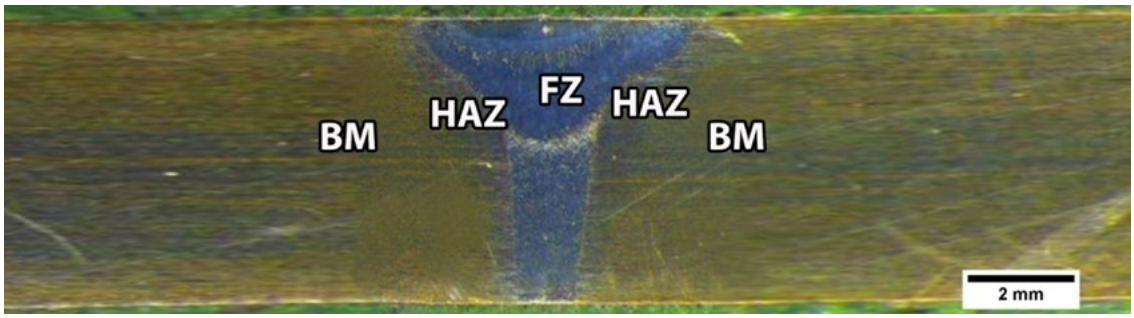

(a) Macrograph of EBW joint

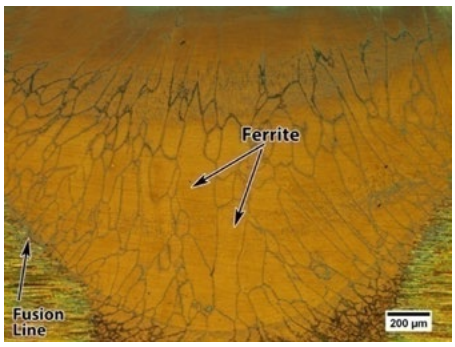

(b) Fusion zone (face side)

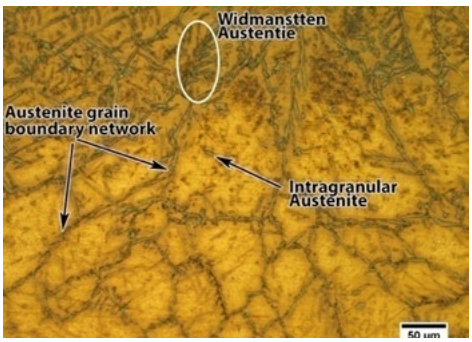

(c) Fusion zone (face side magnified)

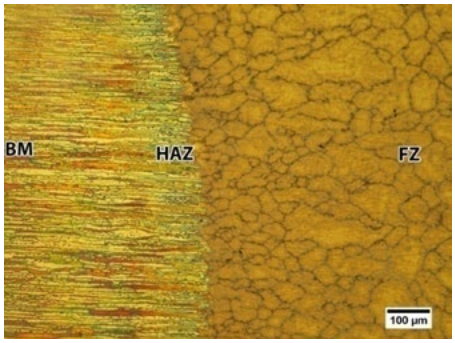

(d) Weld base interface (root side)

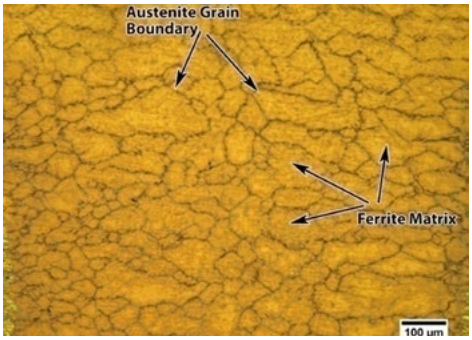

(e) Fusion zone (root side magnified)

Fig.5 - Microstructure of the EBW joint.

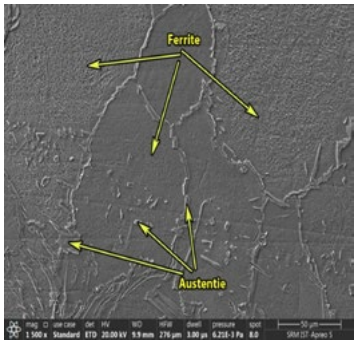

(a) Face side of the fusion zone

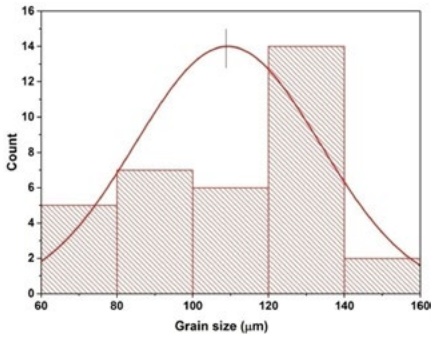

(b) Distribution of grain size (face side)

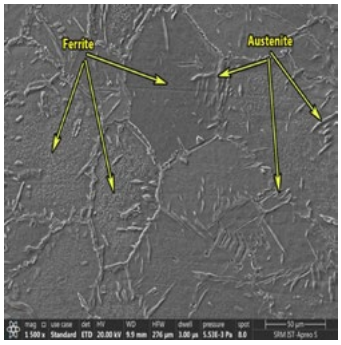

(c) Root side of the fusion zone

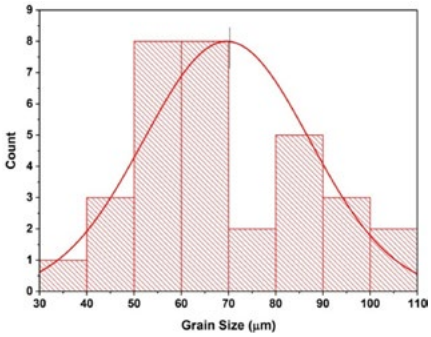

(d) Distribution of grain size (root side)

Fig.6 - Microstructural morphologies of the EBW fusion zone.

FRICTION STIR WELDING (FSW)

The macrostructural characteristics of the FSW joint are displayed in figure 7a. The macrostructure of the FSW joint showed three unique zones: the thermomechanical affected zone at retreating side (TMAZ-RS), the thermo-mechanical affected zone at advancing (TMAZ-AS), and the stir zone (SZ). Because stainless steel has a limited heat conductivity, the heat affected zone (HAZ) is not readily visible in this instance. As a significant large volume of the base metal is mixed by the FSW tool during the joining process, the FSW weld zone produced greater bead width (27.1 mm) and weld area (111.4 mm^2) compared to the EBW joint.

The SZ microstructure of the FSW joint is depicted in figure 7b. Here the SZ microstructure is more significant as compared to the base metal due to the dynamic recrystallization mechanism (DRX). The grain size of the austenite and ferrite phases at the SZ is reduced as compared to the base metal grain thickness due to the severe plastic deformation during the DRX mechanism [17]. The nucleation and growth of the well-refined strain-free grains occurred during the FSW process [18]. Figures 7c and 7d depict the microstructural features of the TMAZ-AS and TMAZ-RS respectively. The distorted grain structure was observed at the TMAZ due to the mechanical deformations due to the heat effect created by the high-speed rotation FSW tool.

The stir zone is magnified in figures 8a and 8b, and the grain size distribution at the stir zone is displayed in figure 8c. Most of the grain size in the stir zone is varying from 5 μm to 14 μm and the average grain size is found as 9 μm. The higher magnification (15000 X, figure 8b) SEM image revealed a distribution of the refined equiaxed ferrite and austenite grains at the center of the stir zone. The formation of the sub grains at the austenite phase indicating that the continuous dynamic recrystallization (CDRX, progressive transformation) occurred at the stir zone [19]. Figures 9a and 9b show magnified views of TMAZ-AS and TMAZ-RS respectively. The presence of the equiaxed grains at the SZ and deformed grains at the TMAZ indicating that the severe plastic deformation occurred at the FS weld zones by the FSW tool [20].

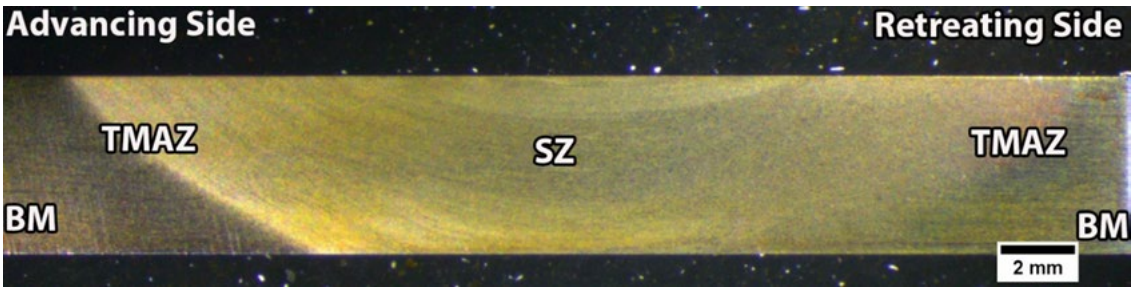

(a) Macrograph of FSW joint

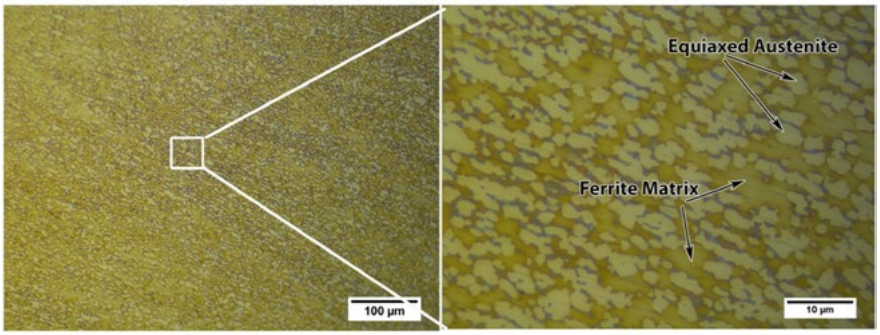

(b) Stir zone

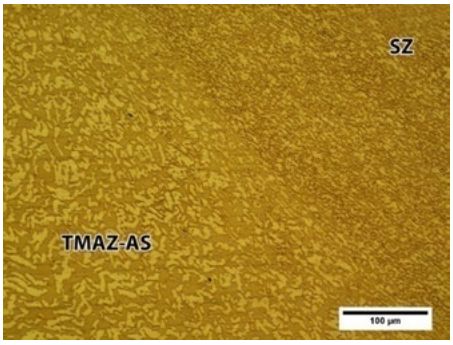

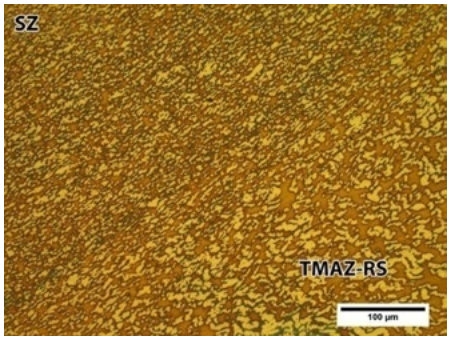

(c) TMAZ-AS

(d) TMAZ-RS

Fig.7 - Microstructure of the FSW Joint (a) Stir Zone (b) TMAZ-AS (b) TMAZ-RS.

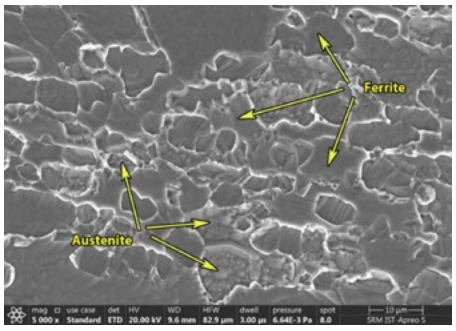

(a) Equiaxed ferrite-austenite grains (stir zone)

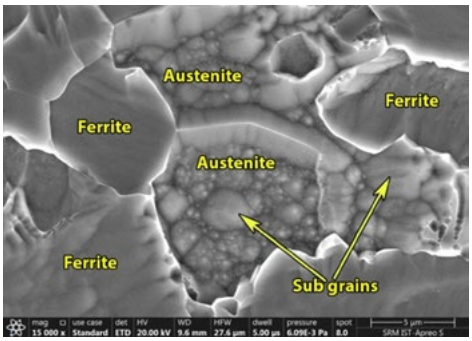

(b) Equiaxed grains (magnified view at the cente of the stir zone)

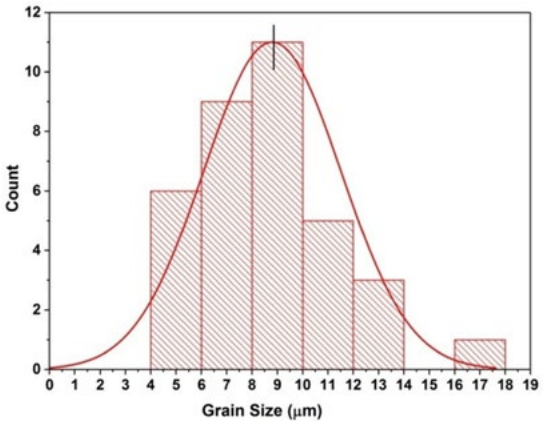

(c) Distribution of the grain size

Fig.8 - Microstructural morphology at the stir zone.

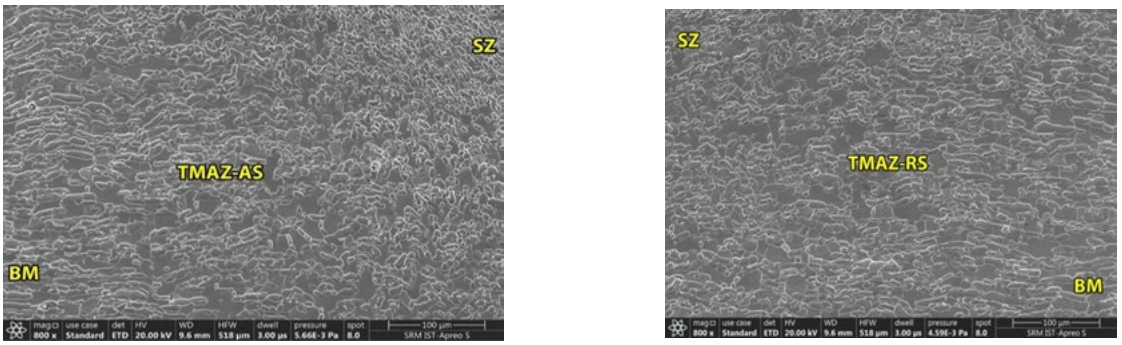

(a) Advancing side **(b)** Retreating side

Fig.9 - Microstructural morphology at the TMAZ of FSW joint.

EVALUATION OF FERRITE CONTENT

Evaluation of the percentage of ferrite phase present in the base metal and weld zones of the different weld joints was done using feritescope. For ferrite measurement, the transverse side of the weld joint was first polished up to 2500 grit emery sheet and then polished using 1 μm diamond paste. Further, the electrolytic etching process was accomplished to reveal the weld zones. A total of four readings were taken at each weld zone (FZ, HAZ) for EBW joints. Similarly, for FSW joint a total of four readings were taken at each zone (SZ, TMAZ-AS and TMAZ-RS) and the average value was calculated. The average percentage of ferrite in the base metal and weld zones were measured using ferrite scope and evaluated values are given in table 4.

Tab.4 - Percentage of ferrite in different weld zones.

Ferrite content in the base metal = 51.2 %			
Welding Process	**Fusion Zone**		**HAZ**
EBW	64.7 ± 0.8		53.9 ± 1.1
	Stir Zone	**TMAZ-AS**	**TMAZ-RS**
FSW	54.6 ± 1.5	58.1 ± 3.1	57.9± 2.2

Microstructural morphologies of the base metal, EBW and FSW joints show the balance between the austenite and ferrite phase with the aid of ferrite measurement. The phase balance is disturbed at the fusion zone of the EBW joint due to the rapid cooling nature. The rapid cooling due to the higher welding speed and narrow fusion zone of the EBW process influenced the formation of the highest amount of the ferrite content in the zone compared to FSW weld zones. The base metal microstructure showed highly elongated austenite and ferrite phases. The EBW fusion zone exhibited two different zones (coarse ferrite grains at the face side and smaller ferrite grains at the root side). The stir zone of the FSW joint showed well-refined strain-free equiaxed grain morphologies of the austenite and ferrite phases due to severe plastic deformation of the dynamic recrystallization phenomenon. The FSW joint exhibited considerably low ferrite content than EBW joints. In the case of the FSW joint, the formation of the higher ferrite content is usually not possible since the joining processes are done without melting and solidification. The fusion zone of the EBW joint has shown the formation of the highest ferrite content compared to the nugget zone of the FSW joint.

MECHANICAL PROPERTIES

Mechanical properties of the duplex stainless steel (DSS) joints are majorly affected by grain morphology and the percentage of ferrite present in the weld zones [21]. The deterioration of the mechanical properties of the DSS and SDSS weld joints is caused by the phase imbalance between ferrite and austenite [22]. A detailed comparison of the primary mechanical properties such as tensile strength,

impact toughness, microhardness and bend properties of the welded joints (EBW and FSW) is presented in this investigation.

TENSILE PROPERTIES

To evaluate transverse tensile properties, three samples of the welded specimens were tested as per the ASTM E8-04 (ASTM 2004). The sub size tensile specimens were prepared and tested in a 100 kN capacity universal testing machine made by MTS (model name MTS Insight). The average values were taken for comparison of the tensile properties. During tensile test for all samples, the cross-shead speed of 1 mm/min was maintained. Figure 10 shows the tensile samples of the welded joints after the experiment. The figure depicts the failure locations of the welded joints after the transverse tensile experiment. The failure location was observed at the fusion zone of the EBW joints. Moreover, failure occurred at SZ and very near to the TMAZ-AS of the FSW joint. Figures 11a and 11b depict the comparison of the stress vs strain curves and evaluated tensile values for the base metal and welded joints. The base metal exhibited yield strength (YS), ultimate tensile strength (UTS) and percentage of elongation of 690 MPa, 825 MPa and 43 % respectively. The superior tensile properties of the FSW joint over EBW joint is due to the following reasons: (1.) formation of the refined equiaxed grains around 9 μm at the stir zone; (2.) formation of the low ferrite content by the action of the solid-state welding phenomenon. The base metal has shown the highest percentage of elongation as compared to all welded joints due to the perfect phase balance between the austenite-ferrite grain morphology. The EBW joint shows the lowest percentage of elongation than the base metal and FSW joints due to the highest ferrite at the fusion zone of the EBW joint [16].

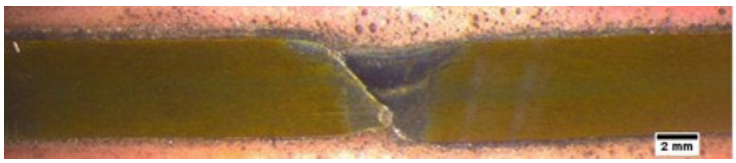

(a) EBW

(b) FSW

Fig.10 - Tensile failure locations of the welded joints.

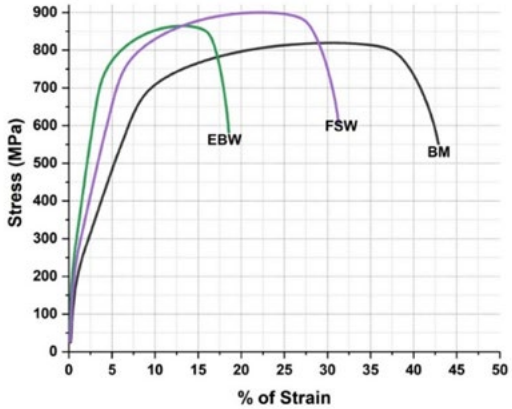

(a) Stress vs strain curve

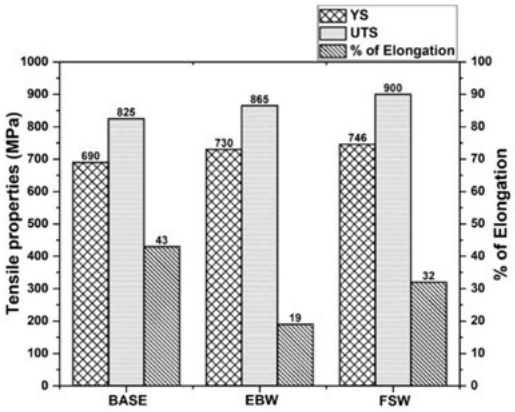

(b) Stress vs strain curve

Fig.11 - Tensile properties of the base metal and welded joints.

FRACTOGRAPHY

The fractography study on the tensile fracture surface was done using a Scanning Electron Microscope (SEM). Figure 12 depicts the tensile fractography of the base metal and welded joints. The presence of dimples and fibrous surfaces in the fracture surface of the base metal indicating the ductile mode fracture (figure 12a). The presence of a few cleavage surfaces indicating a reduction in the ductility of the base metal.

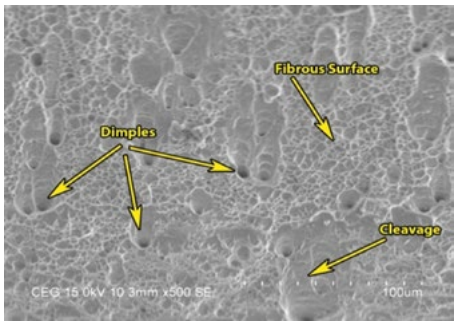

(a) Base metal

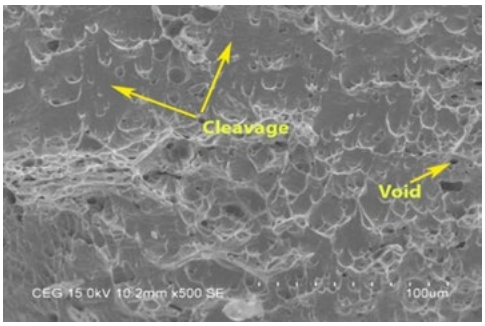

(b) EBW

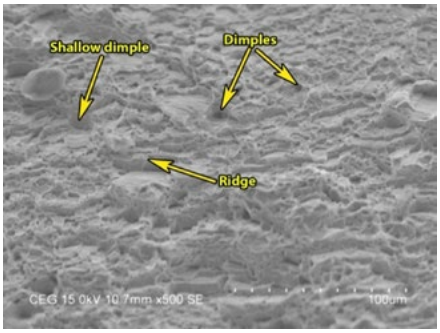

(c) FSW

Fig.12 - Tensile Fractography of the Base metal, EBW and FSW joints.

The major portion of the EBW fracture surface is covered by large cleavage and flat surfaces with considerable voids (figure 12b). This indicates the deterioration of the ductility of the EBW joint as compared to the base metal. In the EBW fusion zone, the austenite-ferrite phase balance is highly affected by the rapid cooling nature due to the narrow electron beam source and higher welding speed. The fracture surface of the FSW joint shows the distribution of fine dimples and microvoids shown in figure 12c. This indicates a higher ductile property of the weld zone at the FSW joint.

MICROHARDNESS

A Vickers microhardness made by Innova Tester (Model 423D) was used to evaluate the microhardness properties of the weld zones. The transverse side of the weld joints was polished up to 2000 grit emery sheet and then the etching was done to reveal the weld zones. A load value of 0.5 Kg and a standard dwell time of 15 sec was used for microhardness measurement study across the transverse side of the weld joints. Throughout the hardness measurement for all weld joints, the distance between the two indentations was maintained as 0.5 mm. Figure 13 depicts the hardness distribution of the transverse side of the EBW joint. The hardness measurement was taken across the face side and root side of the fusion zone. The root side of the fusion zone exhibited a hardness of 315 ± 4 HV and the face side of the fusion zone exhibited a hardness of 300 ± 8. The higher hardness of the root side is attributed to the formation of the smaller ferrite grains as compared to the face side of the fusion zone. Figure 14 shows the distribution of hardness across the FSW weld zone. The hardness of the stir zone varies from 320 HV to 352 HV. This range is quite a bit higher than the base metal and EBW joints. The very fine grain refinement around 9 μm at the stir zone resulted in the highest hardness of the FSW weld zone. However, unsteady microhardness is attributed to the distribution of equiaxed ferrite and austenite morphologies at the stir zone. Because the BCC structure ferrite grains comprise more hardness over FCC structured austenite grains. The TMAZ of the FSW joint showed a hardness range between the base metal and the stir zone.

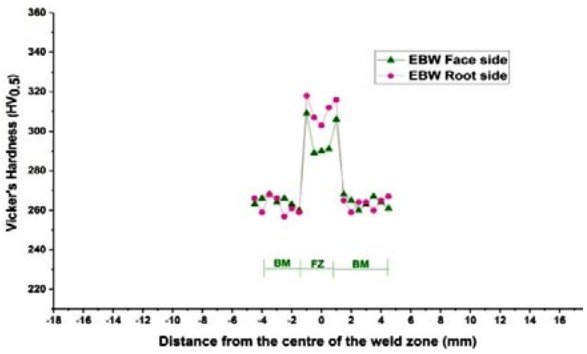

Fig.13 - Distribution of the microhardness of EBW joint.

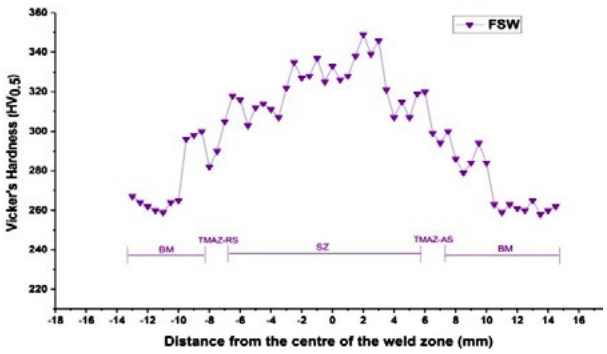

Fig.14 - Distribution of the microhardness of FSW joint.

IMPACT TOUGHNESS

The Charpy impact testing machine made by SANS (Model: ZBC2452-C) was used to assess the toughness of the weld joints. The test was performed at room temperature with a 450 J capacity machine. The Charpy impact test samples before and after the test are shown in figure 15. Figure 16 shows a comparison of the impact toughness values of the base metal and welded joints. The FSW joint showed little reduction in the impact toughness compared to the base metal. The EBW joint showed the lowest impact toughness value due to the formation of high ferrite content (64.7 %).

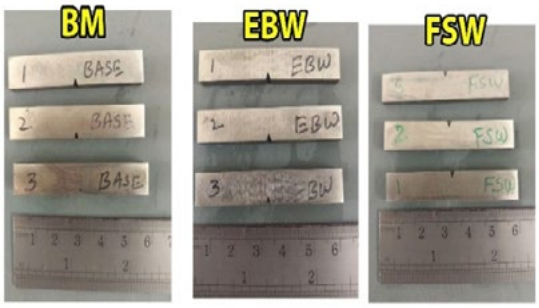

(a) Impact test sample (before the test)

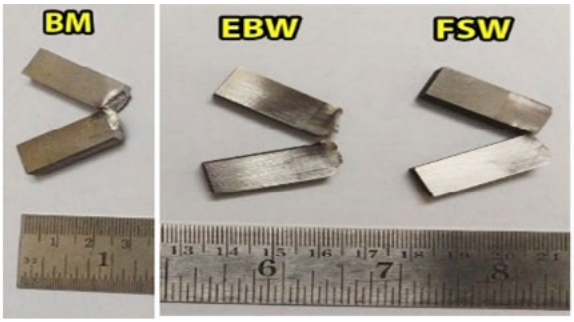

(b) Impact test sample (after test)

Fig.15 - Impact toughness test samples before and after the test.

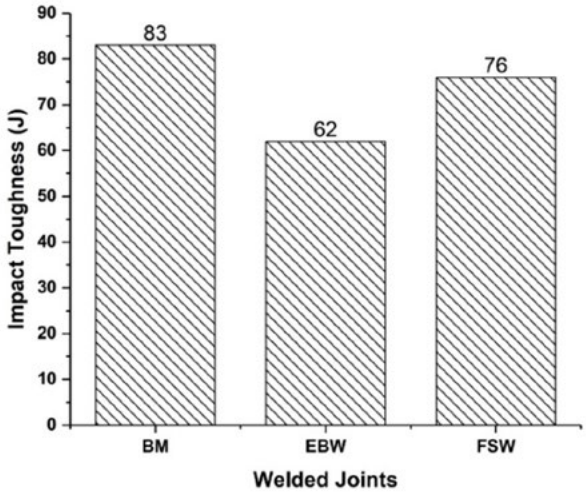

Fig.16 - Impact toughness of base metal and welded joints.

BEND TEST

A 100 kN capacity Universal testing machine made by MTS (model name MTS insight) was used for performing the standard guided 2T bend test for the base metal and weld joints. For the welded joints both face bend and root bend were performed to check the ductility. The bend test samples of different welded joints before and after the experiment are shown in figure 17a and b. The peak load of the base metal and welded joints during the bend test is given in table 5. The bend test results revealed that the base metal and all weld joints are free from cracks, tearings and fissures [23]. The peak load during the face and root bend test for the base metal was observed as 11.74 kN and 10.52 kN respectively. The highest peak load of 13.06 kN was observed for the FSW joint during the face bend experiment. This is attributed to the large portion of the stir zone with well refine austenite and ferrite grains. The lowest peak load of the EBW joint is attributed to the narrow fusion zone with the highest ferrite phase (BCC structured).

Tab.5 - Peak load during the guided bend test.

Peak load for the base metal = 15.32 kN		
Welded Joints	**Peak load during face bend test (kN)**	**Peak load during root bend test (kN)**
EBW	11.41	10.32
FSW	13.06	12.42

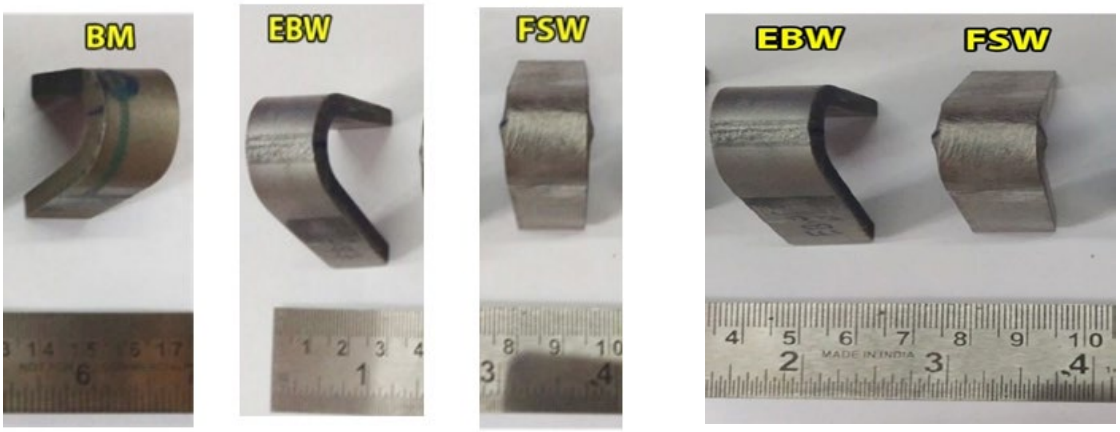

(a) Bend sample (After face bend test) **(b)** Bend sample (After root bend test)

Fig.17 - Bend test for base metal and welded joints.

CONCLUSION

1. Defect free single pass full penetration welds were successfully made on 6mm thick super duplex stainless steel 2507 plates, using Electron Beam and Friction stir welding processes.
2. The ferrite and austenite phase balance changed significantly in EB welds and heat affected zones. The EB weld metal exhibited the highest ferrite content of 64.7 % resulting in higher strength and lower ductility. FS welds showed slightly higher ferrite content compared to the base metal in the nugget zone and TMAZ.
3. The fusion zone of the EBW joint exhibited two different types of grain morphology namely smaller ferrite grains at the root side and coarse ferrite grains at the face side. The different cooling rate at different places is the main reason for the two distinct zones at the EBW fusion zone.
4. The formation of the highest ferrite content (64.7%) at the EBW fusion zone deteriorated the impact toughness property of the EB weld metal.
5. The FSW joints have shown higher yield strength, ultimate tensile strength and percentage of elongation, compared to the EBW joints mainly due to the fine

equiaxed grains in the nugget region of the FS welds, which were caused by dynamic recrystallization.

6. FSW demonstrates superior performance in the bend test than the EB welds, maintaining a higher degree of structural integrity under stress.
7. The FS welds exhibited better ferrite to austenite phase balance at about 55:45, while EB weld metal exhibited a 65:35, which could adversely affect the corrosion resistance of the weld metals.

REFERENCES

[1] J. Anderson, K. Lee, T. Kim, "Corrosion resistance of SDSS 2507 SDSS in marine environments," Journal of Materials Science and Engineering, vol. 56, pp. 254-262, 2017.
[2] A. Vignal, S. Kumar, M. Brown, "Stress and corrosion resistance of duplex stainless steels," Corrosion Science, vol. 130, pp. 112-121, 2018.
[3] V. A. Hosseini, K. Hurtig, L. Karlsson, "Effect of multipass TIG welding on the corrosion resistance and microstructure of a super duplex stainless steel," Materials and Corrosion, vol. 68, no. 4, pp. 405-415, 2017.
[4] M. Sato, Y. Takeda, T. Nakamura, "Electron beam welding and microstructure control in duplex steels," Journal of Manufacturing Processes, vol. 24, pp. 345-354, 2016.
[5] R. Singh, P. Gupta, "Effect of welding techniques on phase balance in duplex stainless steels," Welding Journal, vol. 98, pp. 45-53, 2019.
[6] P., Almeida, L. Silva, R. Costa, "Embrittlement control in SDSS 2507 welded joints," Materials Science and Engineering: A, vol. 783, pp. 116-124, 2021.
[7] Z. Zhang, H. Jing, L. Xu et al., "Influence of heat input in electron beam process on microstructure and properties of duplex stainless steel welded interface," Applied Surface Science, vol. 435, 2018, pp. 352-366.
[8] D. Thomas, H. Kumar, L. Wilson, "Improved joint integrity of duplex steels via FSW," International Journal of Advanced Manufacturing Technology, vol. 105, pp. 3331-3342, 2020.
[9] R. Mishra, Z. Ma, "Overview of friction stir welding for stainless steels," Progress in Materials Science, vol. 92, pp. 234-260, 2019.
[10] L. Chen, M. Zhao, Z. Wang, "Corrosion resistance in FSW duplex stainless steels," Journal of Materials Processing Technology, vol. 293, pp. 117065, 2022.
[11] R. A. Giorjão et al., "Microstructure and mechanical properties of friction stir welded 8mm pipe sdss 2507 super duplex stainless steel," Journal of Materials Research and Technology, vol. 7, Issue 4, 2018, pp. 551-558.
[12] M. M. Seleman et al., "Experimental investigations on mechanical and metallurgical properties of SDSS 2507 welded joints using FSW," International Journal of Integrated Engineering, vol. 14, No. 1, 2022, pp. 1-12.
[13] C. B. Sekar, S. R. Boopathy, S. Vijayan, S. K. Rao, "Effect of GTA welding parameters on bead geometry of SDSS 2507 super duplex stainless steel," La Metallurgia Italiana, n. 9 September, pp. 18-28, 2020, ISSN 0026-0843.
[14] R. Sasidharan, S. R. Boopathy, S. Vijayan, S. K. Rao, "Optimization of bead geometry for duplex stainless steel GTA welds using the Taguchi approach," Mater. Test., vol. 58, no. 4, pp. 312-318, 2016. https://doi.org/10.3139/120.110854.
[15] L. Wang, P. Zhao, J. Pan, L. Tan, K. Zhu, "Investigation on microstructure and mechanical properties of double-sided synchronous TIP TIG arc butt welded duplex stainless steel," The International Journal of Advanced Manufacturing Technology, 112:303-312, 2021.
[16] J. Singh, A. S. Shahi, "Metallurgical and corrosion characterization of electron beam welded duplex stainless steel joints," Journal of Manufacturing Processes, vol. 50, pp. 581-595, 2020.
[17] M. K. Mishra, G. Gunasekaran, A. G. Rao, B. P. Kashyap, N. Prabhu, "Effect of multipass friction stir processing on mechanical and corrosion behavior of 2507 super duplex stainless steel," Journal of Materials Engineering and Performance, vol. 26, no. 2, pp. 849-860, 2017.
[18] H. Sarlak, M. Atapour, M. Esmailzadeh, "Corrosion behavior of friction stir welded lean duplex stainless steel," Materials & Design (1980-2015), 66, 209-216, 2015.
[19] V. A. Hosseini, S. Wessman, K. Hurtig, L. Karlsson, "Nitrogen loss and effects on microstructure in multipass TIG welding of a super duplex stainless steel," Materials & design, vol. 98, pp. 88-97, 2016.
[20] R. S. Mishra, Z. Y. Ma, "Friction stir welding and processing," Materials Science and Engineering R: Reports, vol. 50, issues 1-2, pp. 1-78, 2005.
[21] J. Verma, R. V. Taiwade, "Effect of welding processes and conditions on the microstructure, mechanical properties and corrosion resistance of duplex stainless steel weldments - A review," Journal of Manufacturing Processes, vol. 25, pp. 134-152, 2017.
[22] B. Varbai, T. Pickle, K. Mellinger, "Effect of heat input and role of nitrogen on the phase evolution of 2205 duplex stainless steel weldment," International Journal of Pressure Vessels and Piping, vol. 176, 103952, 2019.
[23] S. Cui, Y. Shi, Y. Cui, T. Zhu, "The impact toughness of novel keyhole TIG welded duplex stainless steel joints," Engineering Failure Analysis, vol. 94, pp. 226-231, 2018.

TORNA ALL'INDICE >